The cosmic microwave background radiation temperature at a redshift of 2.34

R. Srianand*, P. Petitjean†‡ & C. Ledoux§

* *IUCAA, Post Bag 4, Ganeshkhind, Pune 411 007, India*
† *Institut d'Astrophysique de Paris–CNRS, 98bis Boulevard Arago, F-75014 Paris, France*
‡ *CNRS 173–DAEC, Observatoire de Paris-Meudon, F-92195 Meudon Cedex, France*
§ *European Southern Observatory, Karl Schwarzschild Strasse 2, D-85748 Garching bei München, Germany*

The existence of the cosmic microwave background radiation is a fundamental prediction of hot Big Bang cosmology, and its temperature should increase with increasing redshift. At the present time (redshift $z = 0$), the temperature has been determined with high precision to be $T_{CMBR}(0) = 2.726 \pm 0.010$ K. In principle, the background temperature can be determined using measurements of the relative populations of atomic fine-structure levels, which are excited by the background radiation. But all previous measurements have achieved only upper limits, thus still formally permitting the radiation temperature to be constant with increasing redshift. Here we report the detection of absorption lines from the first and second fine-structure levels of neutral carbon atoms in an isolated cloud of gas at $z = 2.3371$. We also detected absorption due to several rotational transitions of molecular hydrogen, and fine-structure lines of singly ionized carbon. These constraints enable us to determine that the background radiation was indeed warmer in the past: we find that $T_{CMBR}(z = 2.3371)$ is between 6.0 and 14 K. This is in accord with the temperature of 9.1 K predicted by hot Big Bang cosmology.

One of the firm predictions of the standard Big Bang model is the existence of relic radiation from the hot phase the Universe experienced at early times[1]. The cosmic microwave background radiation (CMBR) was discovered serendipitously[2] in 1964. The fact that its spectrum follows, with great precision, a planckian distribution over several decades in frequency is a strong argument in favour of the hot Big Bang cosmology. However, the presence of the radiation at earlier times has never been proved directly. The temperature of its black-body spectrum is predicted to increase linearly with redshift $T_{CMBR}(z) = T_{CMBR}(0) \times (1 + z)$ and its local value has been determined very accurately by the Cosmic Background Explorer (COBE) to be $T_{CMBR}(0) = 2.726 \pm 0.010$ K (ref. 3). Detecting the presence of relic radiation at earlier epochs and confirming the well defined predicted temperature evolution is therefore a crucial test for cosmology. To perform this test, we can use the possibility that excited fine-structure levels of the ground-state of atomic species may be partly populated by the cosmic microwave background radiation when the energy separation of the levels is similar to the energy at the peak of the radiation energy distribution.

The relative populations of excited levels can be measured from the absorption lines seen in the spectrum of distant quasars and used to constrain T_{CMBR} at high redshift[4–10]. The expected values make neutral carbon, C^0, particularly suitable for this purpose. The ground term is split into three levels ($J = 0, 1, 2$) with the $J = 0 \rightarrow 1$ and $J = 1 \rightarrow 2$ energy separations kT corresponding to, respectively, $T = 23.6$ and 38.9 K. However, the fine-structure levels can also be excited by collisions (mostly with electrons and hydrogen) and by ultraviolet pumping and following cascades. The ionization potential of neutral carbon, 11 eV, is below the ionization potential of hydrogen, 13.6 eV, and C^0 can only be seen in dense, neutral and highly shielded gas[9]. Therefore, excitation by collisions cannot be neglected.

To constrain T_{CMBR}, the kinetic temperature, the particle density of the gas and the local ultraviolet radiation field must be known. As it is very difficult to disentangle these various excitation processes, all measurements until now have led only to upper limits on T_{CMBR}.

Our measurement was obtained in a unique absorption system where absorption lines of neutral carbon in the three fine-structure levels of the ground term, C^0, $C^{0\star}$ and $C^{0\star\star}$ are observed together with absorption lines of singly ionized carbon in its excited fine-structure level, $C^{+\star}$, and absorption lines of molecular hydrogen (H_2) in the $J = 0$ to 5 rotational levels. The population and depopulation of the first excited rotational level of H_2 ($J = 1$) from and to the ground state ($J = 0$) is controlled by thermal collisions. Therefore the excitation temperature T_{01} is approximately equal to the kinetic temperature. The fine-structure upper level of the C^+ ground-state doublet is mostly populated by collisions and depopulated by radiative decay. Therefore, once the temperature is known, the particle density can be derived from the $C^{+\star}/C^+$ ratio. Finally, the ultraviolet radiation flux can be constrained from the populations of the $J = 4$ and 5 H_2 rotational levels.

Observations

We used the Ultra-violet and Visible Echelle Spectrograph (UVES)[11] mounted on the European Southern Observatory (ESO) KUEYEN 8.2-m telescope at the Paranal observatory on 5 and 7 April 2000, to obtain a high-spectral-resolution spectrum of the quasar PKS1232+0815 with emission redshift $z_{em} = 2.57$ and $m_V = 18.4$. Standard settings have been used in both arms of the spectrograph. Wavelength ranges were 3,290–4,519 Å in the blue and 4,623–5,594 and 5,670–6,652 Å for the red ships. The slit width was 1 arcsec and the charge-coupled devices (CCDs) were binned 2×2 resulting in a wavelength resolution, $\Delta\lambda/\lambda$, of ~45,000. The exposure time was 3 h in seeing conditions better than 0.8 arcsec full-width at half-maximum. The data were reduced using the UVES pipeline in an interactive mode. The pipeline is a set of procedures implemented in the dedicated context of MIDAS, the ESO data reduction package. Its main tasks are to perform a precise inter-order background subtraction for science frames and master flat-fields, and to allow for an optimal extraction of the object signal rejecting cosmic ray

impacts and performing sky-subtraction at the same time. The reduction is checked step by step. Wavelengths are corrected to vacuum-heliocentric values and individual one-dimensional spectra are combined. This resulted in a signal-to-noise (S/N) ratio per pixel of 10 around 3,700 Å and 20 around 6,000 Å. Typical errors in the wavelength calibration are about 0.5 km s^{-1}.

Fit to the lines, metallicity and molecular content

To our knowledge, this is the first time C^0, C^{0*} and C^{0**} absorption lines have been detected at high redshift (see Fig. 1). The detection of these three species at an absorption redshift of $z_{abs} = 2.33771$ is confirmed by the presence of several transitions. C^0 absorption lines with rest wavelengths 1139.79, 1157.91, 1260.73, 1560.31 and 1656.92 Å, C^{0*} absorption lines with rest wavelengths 1194.40, 1279.89, 1329.09, 1329.10, 1329.12, 1560.68, 1560.71, 1656.27, 1657.38 Å and 1657.91 and C^{0**} lines at 1657.00 and 1658.12 Å are clearly detected and are free from any blending with absorption due to other systems. We use the oscillator strengths given by ref. 12 and standard Voigt profile fitting to determine the amount of matter lying on the line of sight and characterized by column densities, N, and the Doppler parameters, $b = \sqrt{b_{th}^2 + b_{turb}^2}$. $b = \sqrt{2k_m T/m}$ is the thermal broadening due to the temperature of the gas, with T the kinetic temperature, k_B Boltzmann's constant and m the mass of the particle; b_{turb} is the turbulent broadening due to macroscopic motions of the gas. Figures 1 and 2 show that the system is dominated by a single, well defined component. We consistently impose the same b value on this component for all species and obtain a best-fit for $b = 1.7 \pm 0.1$ km s^{-1}. This value is small compared to the spectral resolution of the data but is ascertained by the relative optical depths in the numerous lines with very different oscillator strengths. Results are given in Table 1 and the fit to a portion of the spectrum is shown in Fig. 1b and in Fig. 2.

The neutral hydrogen column density in the system, $\log N(H^0) = 20.90 \pm 0.10$, has been obtained by fitting the damped Lyman α line. At such a high column density, hydrogen is mostly neutral and the elements of interest here, iron, magnesium, silicon and carbon, are mainly in the singly ionized state. Column densities are derived from simultaneous Voigt profile fitting of all the available absorption lines using the same Doppler parameter for all species and the same column density for each species. We concentrate however on weak lines, such as $Fe^+\lambda = 1{,}125$, $\lambda = 1{,}608$ and $\lambda = 1{,}611$, $Si^+\lambda = 1{,}808$ or $Mg^+\lambda = 1{,}239$, because they are optically thin. Indeed, in this case, the strength of the line does not depend on the Doppler parameter and gives the column density directly. Profiles of a few transitions are shown on Fig. 2 and results are given in Table 1. The α-chain elements magnesium and silicon have abundances, $Z(X) = N(X)/N(H)$, where X is Mg or Si, that are similar to solar abundances within the measurement uncertainties, $\log Z/Z_\odot \approx -1.2$, where $Z_\odot$ is the solar abundance. However, we note that, relative to the Sun, iron is underabundant by about a factor of 5 compared to silicon and nickel is slightly underabundant compared to iron. If these differences are because iron and nickel are depleted into dust grains, the depletion is of the same order as that observed in warm halo gas in our Galaxy[13]. All this suggests that the system is very much like typical damped Lyman α systems, with metallicity about one tenth of solar and small depletion of iron type element into dust[8,14].

Our echelle data confirms the presence of molecular hydrogen, first detected in ref. 15. At the resolution of the spectrum, most of the H_2 lines are free from blending. The wide wavelength coverage of the spectrum implies that absorption lines from various Lyman bands are seen. Column densities of H_2 in different rotational J levels are obtained by simultaneously fitting various Lyman bands which are free from contamination owing to intervening Lyman α absorption from the diffuse intergalactic medium. Absorption

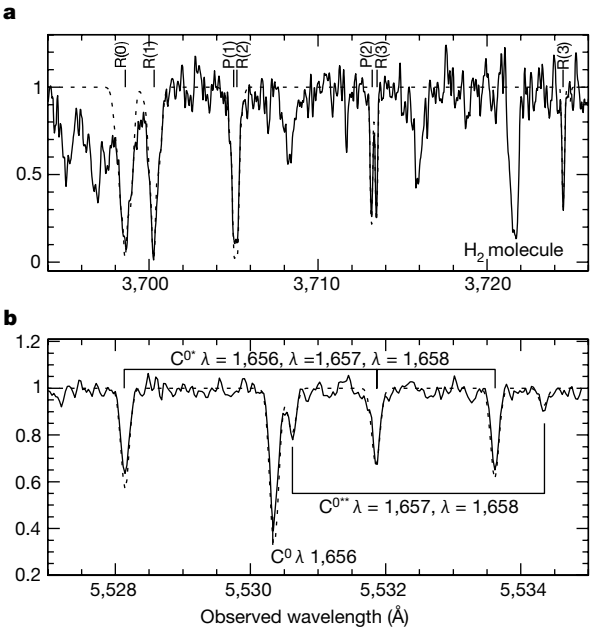

Figure 1 A sample of H_2 and C^0 absorption lines at $z_{abs} = 2.33771$. Portions of the normalized spectrum of the quasar PKS1232+0815 taken with the Ultra-violet and Visible Echelle Spectrograph mounted on the 8.2-m KUEYEN telescope of the European Southern Observatory on the Paranal mountain in Chile. **a**, A selection of H_2 absorption lines from the $J = 0$, 1, 2 and 3 rotational levels from the $v = 0$–1 Lyman band. The model fitted with the parameters given in Table 2 is overplotted to the data as a dashed line. **b**, Detection of absorption lines from C^0, C^{0*} and C^{0**} at $z_{abs} = 2.33771$ in the damped Lyman α system. The model fitted with the parameters given in Table 1 is overplotted to the data as a dashed line.

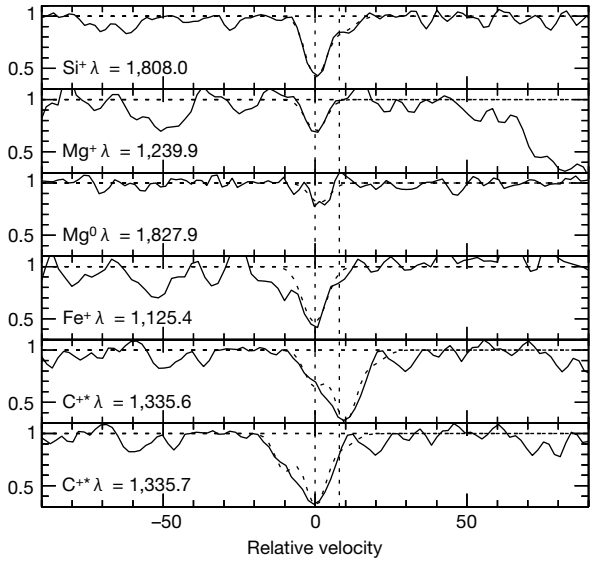

Figure 2 A sample of heavy-element absorption lines at $z_{abs} = 2.33771$. Absorption profiles of a few transitions (indicated on each panel) from the damped Lyman α system toward PKS1232+0815. The normalized flux is given in a velocity scale with origin at $z = 2.33771$. The C^{+*} profile is slightly broader than the other lines. The C^{+*} line is a blend of $C^{+*}\lambda = 1335.71$ and $C^{+*}\lambda = 1335.66$. Fitted models are overplotted as dashed lines. The fit is performed over all the absorption lines available in the spectrum. Our best-fitted column density of 10^{14} cm^{-2} for C^{+*} overpredicts the absorption at $\lambda = 1335.6$.

profiles corresponding to transitions from $J > 1$ rotational levels are consistent with a single component at the same redshift $z_{abs} = 2.33771$ as the C^0 lines. Lines from the $J = 0$ and 1 levels are broader and most of the absorption features have similar profiles, suggesting the presence of several components. We obtain a best fit to these absorption lines with four components. Results of Voigt profile fitting are given in Table 2. The total H_2 column density is $N(H_2) = 1.52 \times 10^{17}\,cm^{-2}$ and the molecular fraction is $f = 2N(H_2)/(2N(H_2) + N(H^0)) = 3.8 \times 10^{-4}$ which is about two orders of magnitude less than what was derived from low dispersion data.

Physical conditions in the gas

In molecular clouds, the kinetic temperature of the gas is given by the excitation temperature, T_{01}, measured between the $J = 0$ and 1 levels. For the components at $z_{abs} = 2.33735$, 2.33754 and 2.33793 we find $T_{01} = 74 \pm 7$, 64 ± 7 K and 66 ± 10 K respectively. None of these components shows detectable absorption due to C^0. The characteristics of the gas are very similar to those measured recently in diffuse gas in the halo of our Galaxy[16]. For the $z_{abs} = 2.3371$ cloud, $T = T_{01} = 185 \pm 100$ K. The excitation temperature T_{ex} for other levels, $J = 2$ to 5, is close to 400 K. This means that processes other than collisions are at play in determining the relative populations of the different levels. Indeed, the $J = 4$ and 5 levels can be populated by cascades following ultraviolet pumping and H_2 formation. We can evaluate the ultraviolet pumping rate from $J = 0$ to $J = 4$, $\beta(0)$, using a simple model[17] and assuming that molecules are formed on dust grains with formation rate R.

$$p_{4,0}\beta(0)n(H_2, J = 0) + 0.19Rn(H)n = A(4 \rightarrow 2)n(H_2, J = 4) \quad (1)$$

where $n = n(H) + 2n(H_2)$, $p_{4,0} = 0.26$ is the pumping efficiency from level $J = 0$ to level $J = 4$. We use the spontaneous transition probabilities $A(4 \rightarrow 2) = 2.8 \times 10^{-9}\,s^{-1}$ as given by ref. 15. Scaling the formation rate of H_2 in our Galaxy ($R \approx 3 \times 10^{-17}\,s^{-1}\,cm^3$) with the dust-to-hydrogen ratio measured in the system ($\leqslant 10^{-1.3}$ the Galactic one) it is easily seen that populating the $J = 4$ level after the formation of a molecule on dust grain is negligible for densities less than $5 \times 10^3\,cm^{-3}$. We estimate the density from the excitation of C^+ to be at least a factor of 100 less than this value (see below). Moreover, for such large densities, the $J = 0$ and $J = 2$ levels as well as the $J = 1$ and $J = 3$ levels should be in thermal equilibrium, which is not the case[19]. We can therefore neglect the population of $J = 4$ and 5 levels by cascades after the formation of a molecule. Finally, we derive from equation (1) that the photo-absorption rate in the Lyman and Werner bands on the surface of the cloud is of the order of $2 \times 10^{-10}\,s^{-1}$, which is quite modest and similar to that observed along sight-lines in our Galaxy[17].

The excited level of the C^+ ground-state term is populated by collisions with electrons and hydrogen atoms[20]. The electrons cannot be neglected because the corresponding collisional cross-section is large. To estimate the electron density we use the ratio $N(Mg^+)/N(Mg^0) = 178$ which is fairly well determined from the detection of the weak lines $Mg^0\lambda = 1{,}737$ and $\lambda = 1{,}827$ and $Mg^+\lambda = 1{,}239$. We have shown (above) that the ionizing flux in the cloud is similar to that observed in our Galaxy, so we can estimate the electron density by equating the Galactic ionizing rate of Mg^0 to the recombination rate of Mg^+ (ref. 12). We find $n_e \approx 0.02\,cm^{-3}$. We note that the electronic density cannot be much smaller than this value because, from the excitation of the $J = 4$ and 5 H_2 levels, we know that the ionizing flux is not smaller than the Galactic value.

Then the hydrogen density can be derived from the $N(C^{+*})/N(C^+)$ ratio. Unfortunately, the $C^+\lambda = 1{,}334$ absorption line is saturated and cannot be used directly to infer $N(C^+)$. We therefore consider that the carbon metallicity can be derived from the silicon metallicity with some correction. Indeed, it is known that the metallicity of the α-chain elements is enhanced compared to carbon by a factor of about two[24] when the mean metallicity is low

Table 1 Heavy elements from the damped Lyman-α system

Ion	log$N$ (cm^{-2})	b (kms^{-1})	[Z/H]	[Z/H] – [Z/H]
H^0	20.90 ± 0.10	–	–	–
C^0	13.86 ± 0.22	1.70 ± 0.10	–	–
C^{0*}	13.43 ± 0.07	–	–	–
C^{0**}	12.63 ± 0.22	–	–	–
C^{+*}	≤14.00	–	–	–
Mg^0	13.19 ± 0.09	–	–	–
Mg^+	15.44 ± 0.09	–	–5.46 ± 0.13	–1.04 ± 0.13
Si^+	15.24 ± 0.11	–	–5.66 ± 0.19	–1.20 ± 0.10
Fe^+	14.68 ± 0.08	–	–6.22 ± 0.13	–1.73 ± 0.13

N is the column density and b is the Doppler width of the line; $b = (2kT/m + b_{turb}^2)^{1/2}$, where m is the atomic mass, T the temperature and b_{turb} the characteristic turbulent velocity of the gas. [Z/H] = log$N(Z)$ – log$N(H_I)$ is the metallicity and [Z/H] – [Z/H]$_\odot$ is the metallicity relative to the value measured in the Sun. We used the solar metallicities from ref. 13. All wavelengths and oscillator strengths are from refs 12 and 28.

Table 2 Fit results to rotational levels in the vibrational ground state of H_2

z_{abs}	Level	log N (cm^{-2})	b ($km\,s^{-1}$)
2.33735	$J = 0$	$3.60 \pm 0.34 \times 10^{15}$	24.07
	$J = 1$	$3.34 \pm 0.40 \times 10^{15}$	24.07 ± 10.20
2.33754	$J = 0$	$4.10 \pm 0.48 \times 10^{15}$	14.09
	$J = 1$	$2.65 \pm 0.44 \times 10^{15}$	14.09 ± 4.57
2.33771	$J = 0$	$2.30 \pm 1.00 \times 10^{16}$	4.62 ± 0.36
	$J = 1$	$8.30 \pm 2.60 \times 10^{16}$	4.62
	$J = 2$	$1.59 \pm 0.27 \times 10^{16}$	4.62
	$J = 3$	$9.39 \pm 1.10 \times 10^{15}$	4.62
	$J = 4$	$4.42 \pm 0.80 \times 10^{14}$	4.62
	$J = 5$	$4.64 \pm 0.77 \times 10^{14}$	4.62
2.33793	$J = 0$	$1.00 \pm 0.04 \times 10^{15}$	21.74
	$J = 1$	$6.69 \pm 0.40 \times 10^{15}$	21.74 ± 1.40

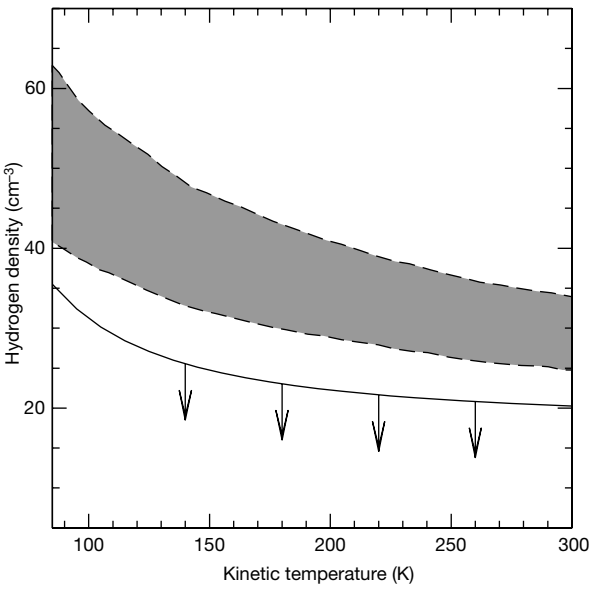

Figure 3 The hydrogen density as a function of kinetic temperature in the $z_{abs} = 2.33771$ cloud. The continuous curve with downward arrows shows the strict upper limit on the hydrogen density estimated from the fine-structure excitation of C^+. The shaded area gives the 2σ range for the hydrogen density required to explain the population ratios in the fine-structure levels of C^0, assuming there is no cosmic background radiation. All other excitation processes (collisions by electrons and hydrogen atoms, ultraviolet pumping) have been taken into account. It is apparent that the observed density is too small to explain the C^0 excitation, demonstrating that the cosmic microwave background radiation (CMBR) exists at $z = 2.33771$.

(that is, ⩽–1.0). To be conservative, we consider that $Z(C) = Z(Si)/2$ and that silicon is not depleted into dust. We note that both assumptions maximize the C^{+*}/C^{+} ratio and, as a consequence, maximize the derived hydrogen density, n_H. In addition, the very small C^0/C^+ value shows that the ionization correction is negligible. Also, the absorptions due to Si^{3+} and C^{3+} are unusually weak in this damped system. The fit of the $C^{+*}\lambda = 1{,}335.6$ and $\lambda = 1{,}335.7$ lines is shown in Fig. 2. The observed C^{+*} profile suggests the presence of possible extra components. Our measured column density is therefore an upper limit which will become an upper limit on the hydrogen density. The strongest constraint comes from the $\lambda = 1{,}335.6$ line in the blue wing of the profile.

Results on the determination of n_H are presented in Fig. 3. For a kinetic temperature in the range $85 < T < 285$ K, as suggested from the H_2 absorption, we find $20 < n_H < 35\,cm^{-3}$ (solid curve on Fig. 3). All the above assumptions maximize the hydrogen density, which can therefore be considered for each temperature as a conservative upper limit.

Cosmic microwave background radiation temperature

The fine-structure levels of C^0 can be populated by several processes, mainly collisions with hydrogen atoms and electrons, and pumping due to the local ultraviolet radiation and to the CMBR. The different contributions can be estimated once the temperature and the particle density are known. We have derived above $85 < T < 285$ K, $20 < n_H < 35\,cm^{-3}$ and $n_e/n_H \approx 0.001$, where n_e is the electron density.

Following ref. 5 and using cross-sections given in refs 22 and 23, we investigate the fine-structure excitation of C^0, keeping the particle density and the temperature within the ranges we determined. For a radiation field similar to that of the Milky Way[24], the ultraviolet pumping rate from the ground state to the excited states of C^0 is $7.55 \times 10^{-10}\,s^{-1}$. The corresponding value for the hydrogen collisional rate in the density and temperature ranges considered here is of the order of $\sim 1.2–1.4 \times 10^{-8}\,s^{-1}$. Thus the contribution due to ultraviolet pumping is negligible. Keenan *et al.*[25] noticed that collisions with electrons are unimportant for kinetic temperatures in the range 100–500 K and a ratio of electron density to hydrogen density that is less than 0.01. Collisions with electrons can therefore be neglected.

The observed 2σ range for $N(C^{0*})/N(C^0)$ and $N(C^{0**})/N(C^0)$ are, respectively, 0.28–0.48 and 0.020–0.060. Assuming collision by hydrogen atoms is the only process at work, we estimate the range of hydrogen density needed to explain the C^0 populations. This density range is shown as a shaded region in Fig. 3. It is apparent that the observed upper limit on the hydrogen density derived above is not sufficient to populate the excited fine-structure levels of C^0 and that an additional source of excitation is needed. The only process we are left with is direct pumping due to photons from the relic background radiation.

We estimate the allowed range for the CMBR temperature as a function of kinetic temperature, after taking into account all previously discussed processes. The allowed area in the T_{CMBR}–T plane is shown as the shaded region in Fig. 4. This region is obtained using the upper limit on the hydrogen density derived above and the 2σ ranges of the C^{0*}/C^0 and C^{0**}/C^0 ratios. Thus the lower T_{CMBR} border of this area gives a stringent lower limit on the CMBR temperature at $z_{abs} = 2.33771$.

We note that an upper limit on T_{CMBR} is obtained by assuming that the CMBR is the only excitation process at work. This limit is shown as a dotted line in Fig. 4.

The presence of a relic radiation field at any redshift is more or less generally accepted in the literature. But its reality has been proved observationally only in the local universe through direct measurements[3,26] and the Sunyaev & Zeldovich effect[27]. Our measurement demonstrates for the first time, to our knowledge, that the

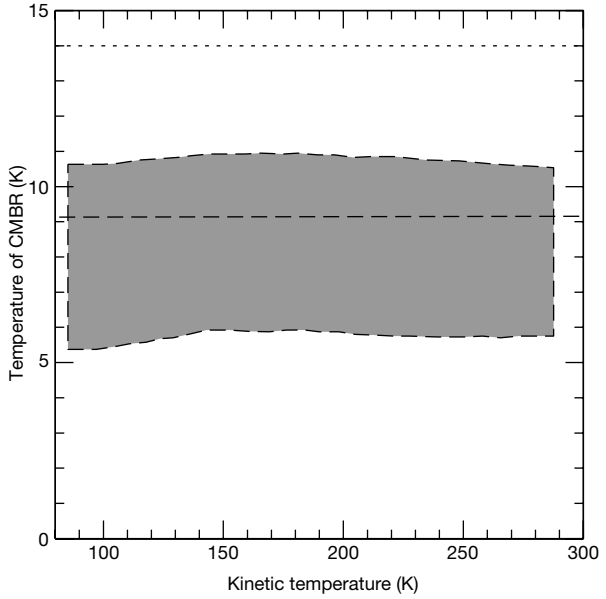

Figure 4 Cosmic microwave background temperature as a function of kinetic temperature of the gas. For a given temperature, we obtain an upper limit of the hydrogen density from the C^+ fine-structure population. This is used to derive the contribution of hydrogen collisions to the C^0 fine-structure excitation. The excess is used to determine the range for the CMBR temperature. The shaded region gives the 2σ range of the CMBR radiation temperature allowed by the observed population ratios of neutral carbon fine-structure levels. The horizontal dotted line is the upper limit on T_{CMBR} if CMBR is assumed to be the only excitation process. The dashed line is the predicted temperature at $z = 2.33771$ in the standard Big Bang model. This demonstrates the presence of a background radiation with a temperature at least twice that measured in the local universe, $T_{CMBR,0} = 2.726$ K.

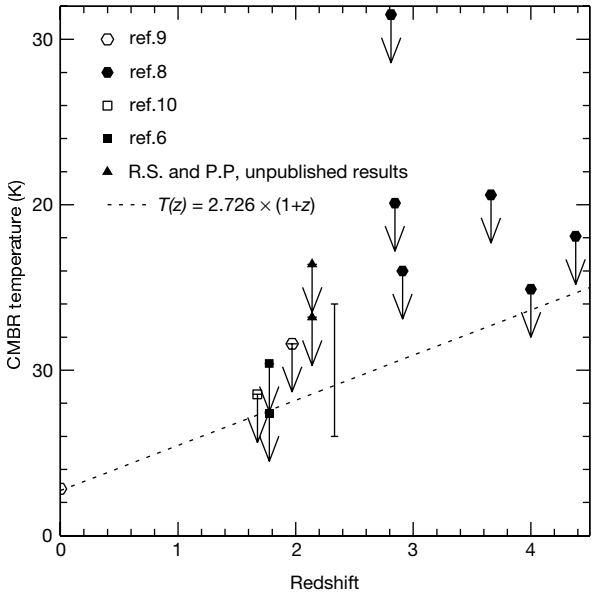

Figure 5 Measurements of the cosmic microwave background radiation temperature at various redshifts. The point at $z = 0$ shows the result of the Cosmic Background Explorer (COBE) determination[3], $T_{CMBR}(0) = 2.726 \pm 0.010$ K. Upper limits are previous measurements[3,8–10] using the same techniques as we did. We also include our two new unpublished upper limits at $z = 2.1394$ along the line of sight toward Tololo 1037–270. The measurement from this work, $6.0 < T_{CMBR} < 14.0$ K at $z = 2.33771$, is indicated by a vertical bar. The dashed line is the prediction from the hot Big Bang, $T_{CMBR}(z) = T_{CMBR}(0) \times (1 + z)$.

cosmic radiation exists at earlier times and has a higher temperature than today. In the standard Big Bang cosmology the cosmic microwave background is a relic radiation left over from an early hot phase. In such a model the radiation evolves adiabatically in the expanding universe and the temperature at any redshift is simply $T(z) = T(z = 0)(1 + z)$. We summarize all the available upper limits in Fig. 5, together with our measurement. The prediction for the adiabatic expansion is shown as a dotted line. These upper limits and our measurements are consistent with the predictions of the standard model. Similar analysis over a large redshift range will provide a direct, model-independent measure of the evolution of the cosmic microwave background radiation. □

Received 7 August; accepted 3 November 2000.

1. Alpher, R. A., Bethe, H. A. & Gamov, G. Evolution of chemical elements. *Phys. Rev.* **73,** 803–804 (1948).
2. Penzias, A. A. & Wilson, R. A measurement of excess antenna temperature at 4080 Mc/s. *Astrophys. J.* **142,** 419–421 (1965).
3. Mather, J. C. *et al.* Measurement of the cosmic microwave background spectrum by the COBE FIRAS instrument. *Astrophys. J.* **420,** 439–444 (1994).
4. Bahcall, J. N., Joss, P. C. & Lynds, R. On the temperature of the microwave background radiation at a large redshift. *Astrophys. J.* **182,** L95–L98 (1973).
5. Meyer, D. M., Black, J. H., Chaffee, F. H., Foltz, C. B. & York, D. G. An upper limit on the microwave background temperature at $z = 1.776$. *Astrophys. J.* **308,** L37–L41 (1986).
6. Songaila, A. *et al.* Measurement of the microwave background temperature at a redshift of 1.776. *Nature* **371,** 43–45 (1994).
7. Songaila, A., Cowie, L. L., Hogan, C. & Rugers, M. Deuterium abundance and background radiation temperature in high redshift primordial clouds. *Nature* **368,** 599–604 (1994).
8. Lu, L., Wargent, W. L. W., Womble, D. S. & Barlow, T. A. Abundances at high redshifts: The chemical enrichment history of damped Lyman-α galaxies. *Astrophys. J. Suppl. Ser.* **107,** 475–520 (1996).
9. Ge, J., Bechtold, J. & Black, J. H. A new measurement of the cosmic microwave background radiation temperature at $z = 1.97$. *Astrophys. J.* **474,** 67–73 (1997).
10. Roth, K. C. & Bauer, J. M. The $z = 1.6748$ C I absorber toward PKS 1756+237. *Astrophys. J.* **515,** L57–L60 (1999).
11. D'odorico, S. *et al.* Performance of UVES, the echelle spectrograph for the ESO VLT and highlights of the first observations of stars and quasors. *Proc. SPIE* **4005,** 121–130 (2000).
12. Welty, D. E. *et al.* The diffuse interstellar cloud toward 23 Orionis. *Astrophys. J. Suppl. Ser.* **124,** 465–501 (1999).
13. Savage, B. D. & Sembach, K. R. Interstellar abundances from absorption-line observations with the Hubble space telescope. *Annu. Rev. Astron. Astrophys.* **34,** 279–330 (1996).
14. Pettini, M., Smith, L. J., King, D. L. & Hunstead, R. W. The metallicity of high-redshift galaxies: the abundance of zinc in 34 damped Lyman-α systems from $z = 0.7$ to 3.4. *Astrophys. J.* **486,** 665–680 (1997).
15. Ge, J. & Bechtold, J. in *Highly Redshifted Radio Lines* (eds Carilli, C. L., Radford, S. J. E., Menten, K. M. & Langston, G. I.) 121–131 (ASP Conf. Series Vol. 156, 1999).
16. Shull, J. M. *et al.* FUSE observations of diffuse interstellar molecular hydrogen. *Astrophys. J.* **538,** L73–L76 (2000).
17. Jura, M. Interstellar clouds containing optically thick H_2. *Astrophys. J.* **197,** 581–586 (1975).
18. Dalgarno, A. & Wright, E. L. Infrared emissivities of H_2 and HD. *Astrophys. J.* **174,** L49–L51 (1972).
19. Srianand, R. & Petitjean, P. Molecules in the $z_{abs} = 2.8112$ damped system toward PKS 0528-250. *Astron. Astrophys.* **335,** 33–40 (1998).
20. Bahcall, J. N. & Wolf, R. A. Fine-structure transitions. *Astrophys. J.* **152,** 701–729 (1968).
21. Timmes, F. X., Lauroesch, J. J. & Truran, J. W. Abundance histories of QSO absorption systems. *Astrophys. J.* **518,** 468–476 (1995).
22. Nussbaumer, H. & Rusca, C. Forbidden transitions in the C I sequence. *Astron. Astrophys.* **72,** 129–133 (1979).
23. Launay, J. M. & Roueff, E. Fine structure excitation of carbon and oxygen by atomic hydrogen impact. *Astron. Astrophys.* **56,** 289–292 (1977).
24. Jenkins, E. B. & Shaya, E. J. A survey of interstellar C I insight on carbon abundances UV grain albedoes, and pressures in the interstellar medium. *Astrophys. J.* **231,** 55–72 (1979).
25. Keenan, F. P., Lennon, D. J., Johnson, C. T. & Kingston, A. E. Fine structure population for the 2P ground states of C II. *Mon. Not. R. Astron. Soc.* **220,** 571–576 (1986).
26. Roth, K. C. & Meyer, D. M. Cyanogen excitation in diffuse interstellar cloud. *Astrophys. J.* **441,** 129–143 (1995).
27. Sunyaev, R. A. & Zeldovich, Ya. B. The velocity of clusters of galaxies relative to the microwave background—The possibility of its measurement. *Mon. Not. R. Astron. Soc.* **190,** 413–420 (1980).
28. Morton, D. C. Atomic data for resonance absorption lines. I—Wavelengths longward of the Lyman limit. *Astrophys. J. Suppl. Ser.* **77,** 119–202 (1991).

Acknowledgements

The observations presented here have been obtained using the Ultra-violet and Visible Echelle Spectrograph mounted on the 8.2-m KUEYEN telescope operated by the European Southern Observatory at Paranal, Chile. P.P. thanks A. Kaufer and M. Chadid for their kind and efficient assistance at the telescope and IUCAA for hospitality during the time this work was being done. We thank T. Padmanabhan for useful comments. We gratefully acknowledge support from the Indo-French Centre for the Promotion of Advanced Research (Centre Franco-Indien pour la Promotion de la Recherche Avancée).

Correspondence and requests for materials should be addressed to R.S. (e-mail: anand@iucaa.ernet.in).